(Preprint) AAS 18-289

DISPOSAL TRAJECTORIES FROM NEAR RECTILINEAR HALO ORBITS

Kenza K. Boudad[*], Diane C. Davis[†], and Kathleen C. Howell[‡]

After completion of a resupply mission to NASA's proposed Lunar Orbital Platform - Gateway, safe disposal of the Logistics Module is required. One potential option is disposal to heliocentric space. This investigation includes an exploration of the trajectory escape dynamics from an Earth-Moon Near Rectilinear Halo Orbit (NRHO) and applies these insights to the design of a low-cost heliocentric Logistics Module disposal option. The effects of the solar gravitational perturbations are assessed in both the bicircular restricted 4-body problem and in an ephemeris force model.

INTRODUCTION

The proposed Lunar Orbital Platform - Gateway is the current framework for the NASA development of a space facility near the Moon with an option to return to the lunar surface.[1,2] From a baseline trajectory concept in a Near Rectilinear Halo Orbit (NRHO), the Gateway is intended to serve as a proving ground for deep space technologies and as a staging location for missions beyond cislunar space. The Orion spacecraft is planned to transport crew to the Gateway, with resupply missions executed by one or more Logistics Modules (LM).[1] After completion of a resupply mission, safe disposal of the LM is required, and one potential option is disposal to heliocentric space.

The NRHO and a sample disposal trajectory appear in Figure 1. The current investigation includes exploration of the trajectory escape dynamics from an NRHO and leverages these insights to the design of a heliocentric LM disposal option. The perturbing effects of the Sun on the LM orbit as it escapes from the Earth-Moon NRHO are critical to any heliocentric disposal design. The solar gravitational perturbations are assessed in both the Bicircular Restricted 4-Body Problem (BCR4BP) and an ephemeris force model. To successfully reach heliocentric space along an escape path, solar orientation (epoch) and energy level are key contributors. To assess their impact, this analysis suggests departure criteria and illustrates the results via sample scenarios.

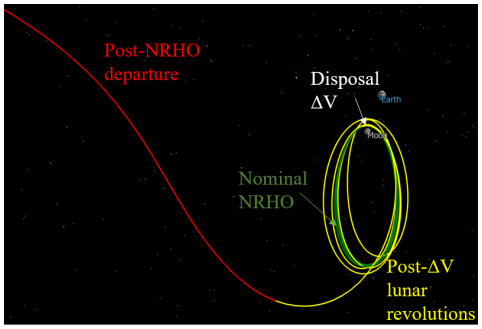

Figure 1: **Sample NRHO disposal trajectory as viewed in the Earth-Moon rotating frame.**

DYNAMICAL MODELS

In this investigation of a vehicle disposal from an Earth-Moon NRHO, the Bicircular Restricted 4-Body Problem (BCR4P) and a higher-fidelity ephemeris model serve as the dynamical bases for the analysis. The

[*]Graduate Student, School of Aeronautics and Astronautics, Purdue University, Armstrong Hall of Engineering, 701 W. Stadium Ave., West Lafayette, IN 47907-2045 kboudad@purdue.edu.

[†]Principal Systems Engineer, a.i.solutions, Inc., 2224 Bay Area Blvd, Houston TX 77058, diane.davis@ai-solutions.com.

[‡]Hsu Lo Distinguished Professor, School of Aeronautics and Astronautics, Purdue University, Armstrong Hall of Engineering, 701 W. Stadium Ave., West Lafayette, IN 47907-2045, howell@purdue.edu. Fellow AAS; Fellow AIAA

BCR4P incorporates the influence of solar gravity on the Earth-Moon-spacecraft three-body system and offers an increase in fidelity over the Circular Restricted 3-Body Problem (CR3BP). A higher-fidelity N-body model, based on ephemeris data, accommodates additional forces and perturbations as modeled in the FreeFlyer software package. Numerical simulations in the ephemeris model are necessary but generally time-consuming and inefficient without sufficient insight into the behavior under the multiple gravitional influences. The use of the BCR4BP therefore avoids increased complexity but captures the most significant influences on the behavior. Suitable disposed trajectories obtained in the BCR4BP are then transitioned to the higher-fidelity ephemeris model.

The Bicircular Restricted Four-Body Problem

The BCR4BP[3] incorporates the gravitational impact of three massives bodies, for instance, the Earth E, the Moon M and the Sun S, on the motion of a spacecraft P. The mass of P is assumed to be negligible in comparison to the masses of the other bodies. Denote Earth and the Moon as the primary bodies. The Earth and the Moon are assumed to move in a circular orbit around their common barycenter B_1 as defined in Figure 2. The Sun and B_1 then move in circular orbits around the $E-M-S$ system barycenter B_2. As apparent in Figure 2, the plane of Earth-Moon primary motion and the Sun orbital plane are not assumed to be coplanar in this model. This BCR4BP model is not coherent since the motions of the primaries and the Sun are not a solution of the general 3BP. Coherent restricted 4-body models have been the subject of other investigations[4,5] but the additional complexity is not necessary for this analysis. In addition to the inertial frame, two rotating frames are defined in Figure 2. An Earth-Moon (E-M) rotating frame is fixed such that $\hat{x}$ axis lies along the Earth-Moon line, the $\hat{z}$ axis is aligned with primaries' orbital angular momentum, and the $\hat{y}$ axis completes the right-handed orthonormal set. The solar orbital plane is defined by the inclination i with respect to the Earth-Moon plane and the longitude Ω of the Sun's ascending node along its orbit. The second rotating frame, Sun-B_1 is fixed in the motion of the Sun and B_1 the Earth-Moon barycenter. The $\hat{x}'$ axis is defined such that it is along the line joining the Sun to B_1 $\hat{z}'$ is aligned with the Sun and B_1 angular momentum vector, and $\hat{y}'$ completes the right-handed orthornomal set.

The differential equations governing motion in the BC4BP are derived by adding the solar gravity influence to the Earth-Moon CR3BP. The Sun angle, θ_S, is the angle between the projection of the rotating $\hat{x}$ axis on the Sun orbital plane and the Sun position vector relative to B_1 and is linearly decreasing: $\theta_S = -\omega_S\, t$. The position vector for P, $\bar{x}^{\alpha}_{\beta}$, is expressed as a row vector in the frame α with respect to the basepoint β. The direction cosine matrix that rotates row position vectors from the $E-M$ rotating frame to the $S-B_1$ rotating frame is defined as follows,

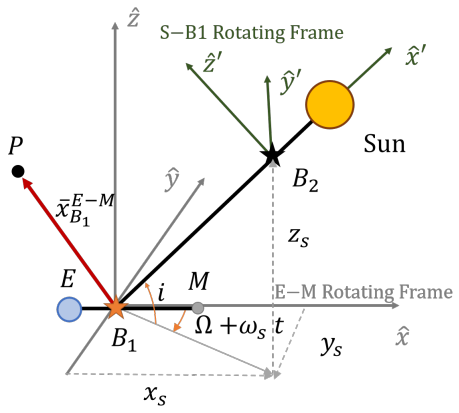

Figure 2: Frames and vectors definitions in the BCR4BP

$$\bar{x}^{S-B_1 \text{ Rotating}}_{B_1} = \bar{x}^{E-M \text{ Rotating}}_{B_1}\,\mathbf{A} \qquad (1)$$

where

$$\mathbf{A} = \begin{bmatrix} \cos(\Omega) & -\sin(\Omega) & 0 \\ \sin(\Omega) & \cos(\Omega) & 0 \\ 0 & 0 & 1 \end{bmatrix} \begin{bmatrix} 1 & 0 & 0 \\ 0 & \cos(i) & -\sin(i) \\ 0 & \sin(i) & \cos(i) \end{bmatrix} \begin{bmatrix} \cos(-(\theta_S-\Omega)) & \sin(-(\theta_S-\Omega)) & 0 \\ -\sin(-(\theta_S-\Omega)) & \cos(-(\theta_S-\Omega)) & 0 \\ 0 & 0 & 1 \end{bmatrix} \qquad (2)$$

For computational purposes, the states in the BCR4BP are nondimensionalized using characteristic quantities. The characteristic mass m^* is the sum of the masses of Earth and the Moon. The characteristic distance l^* is the distance between the Earth and the Moon and is assumed constant. Choosing the nondimensional

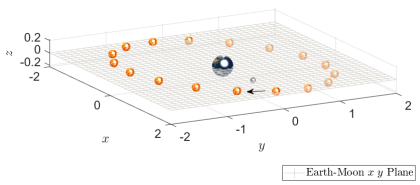

Figure 3: **Sun's orbit (not to scale) as viewed in the Earth-Moon Rotating Frame**

angular motion of E and M to be equal to one yields the nondimensional characteristic time t^*. The Sun's mass, m_S, its distance from the Earth-Moon barycenter (B_1), a_S, and the solar angular velocity with respect to the Earth-Moon rotating frame, w_S, are nondimensional values defined with the characteristic quantities. The nondimensional mass parameter μ is defined as the mass of the Moon over the characteristic mass, m^*. The equations of motions of the BCR4BP are

$$\begin{aligned}
\ddot{x} &= 2\dot{y} + x - \frac{(1-\mu)(x+\mu)}{r_{13}^3} - \frac{\mu(x-1+\mu)}{r_{23}^3} - \frac{m_s(x-x_s)}{r_{s3}^3} - \frac{m_s}{a_s^3}x_s \\
\ddot{y} &= -2\dot{x} + y - \frac{(1-\mu)y}{r_{13}^3} - \frac{\mu y}{r_{23}^3} - \frac{m_s(y-y_s)}{r_{s3}^3} - \frac{m_s}{a_s^3}y_s \\
\ddot{z} &= -\frac{(1-\mu)z}{r_{13}^3} - \frac{\mu z}{r_{23}^3} - \frac{m_s(z-z_s)}{r_{s3}^3} - \frac{m_s}{a_s^3}z_s
\end{aligned} \tag{3}$$

where x, y and z are the components of $\bar{x}_{B_1}^{E-M \text{ Rotating}}$, the distance from P to Earth is labeled r_{13} and $r_{13} = \sqrt{(x+\mu)^2 + y^2 + z^2}$, the distance from P to the Moon is $r_{23} = \sqrt{(x-1+\mu)^2 + y^2 + z^2}$. The Sun's position vector with respect to the Earth-Moon barycenter B_1 is then,

$$\bar{r}_S = \begin{bmatrix} x_S \\ y_S \\ z_S \end{bmatrix}^T = \begin{bmatrix} a_s \left(\cos(\theta_s - \Omega)\cos(\Omega) \;\; -\sin(\theta_s - \Omega)\;\sin(\Omega)\;\cos(i) \right) \\ a_s \left(\cos(\theta_s - \Omega)\sin(\Omega) \;\; +\sin(\theta_s - \Omega)\;\cos(\Omega)\cos(i) \right) \\ a_s \;\sin(\theta_s - \Omega)\sin(i) \end{bmatrix}^T \tag{4}$$

where the superscript T indicates the transpose of a vector. Equations 3 and 4 describe the motion of the spacecraft P in the under the influence of the Earth, the Moon, and the Sun in the E-M rotating frame and expressed in nondimensional quantities.

The BCR4BP explicitly depends on time and therefore does not possess an integral of the motion. Thus, the energy for P in the BCR4BP is not conserved. However, its instantaneous values offer insights concerning the dynamical flow by unveiling instantaneous forbidden region and instantaneous equilibrium points. The energy can be defined in different frames: rotating Earth-Moon or rotating Sun-B_1 and with respect characteristic quantities. In the Earth-Moon rotating frame, the instantaneous energy E is defined as :

$$E = x^2 + y^2 + 2\frac{1-\mu}{r_{13}} + 2\frac{\mu}{r_{23}} + 2\frac{m_S}{r_{S3}} - 2\frac{m_S}{a_S^3}\left(x_S x + y_S y + z_S z\right) - (\dot{x}^2 + \dot{y}^2 + \dot{z}^2) \tag{5}$$

In the S-B_1 rotating frame, the energy H is:

$$H = x'^2 + y'^2 + 2\frac{m_S - 1}{m_S\, r'_{S3}} + 2\frac{\mu}{m_s\, r'_{13}} + 2\frac{\mu}{m_S\, r'_{23}} - (\dot{x'}^2 + \dot{y'}^2 + \dot{z'}^2) \tag{6}$$

where x', y' and z' are the components of the position vector from $E - M - S$ system barycenter B_2, $\bar{x}_{B_2}^{S-B_1 \text{ Rotating}}$, in the $S - B_1$ rotating frame; x', y' and z' are the components of the velocity vector in the same frame, and r'_{S3}, r'_{13} and r'_{23} are the norms of the primary-to-spacecraft vectors in the $S - B_1$ rotating frame. Note that E is computed using the state nondimensionalized with the E-M characteristic quantities, while H, the energy in the S-B_1 frame, is computed using the state nondimensionalized with respect to the CR3BP S-B_1 characteristic quantities.

Instantaneous equilibrium points exist in the BCR4BP. In the Earth-Moon vicinity, they correspond to the CR3BP E-M L_i equilibrium points perturbed by the Sun. Away from the Earth-Moon system, the CR3BP S-B_1 L'_i are perturbed by the orbital motions of the Earth and the Moon. Using the CR3BP L_i as an initial guess and using a differential correction process, the BCR4BP instantaneous equilibrium points

are straightforwardly located. At every instant, the locations shift due to the orientation of the Sun. Simultaneously, the value of the energy is also changing which impacts an instantaneous set of zero velocity curves. Access to regions surrounding the Earth and the Moon through the Sun-B_1 L_1 and L_2 opening is summarized in Figure 4 for different solar orientations. Such information serves as a guide in assessing departure to heliocentric space.

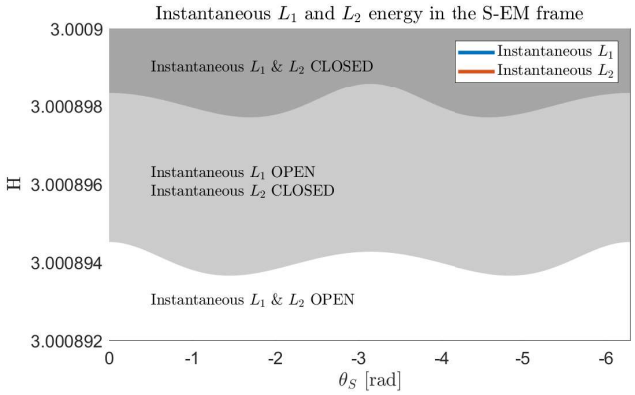

Figure 4: **Instantaneous L_1 and L_2 energy in the BCR4BP**

The Ephemeris Model

For applications in mission scenarios where high-fidelity modeling accuracy is required, N-body differential equations and planetary ephemerides are employed. The N-body dynamics generally render the motion of a particle of interest (e.g., a spacecraft) in an inertial frame relative to a central body under the gravitational influence of the same central body and other additional perturbing bodies. Within this analysis, the relative position of each perturbing body with respect to the central body is instantaneously computed by employing NAIF SPICE ephemeris data. The Moon is selected as the central body for numerical integration in the J2000 inertial frame. The Earth and Sun are included as point masses, and the Moon's gravity is modeled using the GRAIL (GRGM660PRIM) model truncated to degree and order 8. Solar radiation pressure (SRP) is also included in the force model.

Operational errors on the spacecraft are considered in the higher-fidelity modeling. For multi-revolution propagations prior to a disposal maneuver, orbit maintenance maneuvers (OMMs) are implemented, and each OMM is associated with a navigation error on the spacecraft state of 10 km in position and 10 cm/s in velocity and a maneuver execution error of 1.5% in magnitude, 1° in direction, and a fixed component of 1.42 mm/s. Mismodeling in SRP assumptions provide 15% error in area and 30% error in coefficient of reflectivity. Momentum wheel desaturations are assumed to occur once per revolution near apolune with a translational Δv component of 3 cm/s. All values are 3σ and are implemented as Gaussian errors with zero mean.

NRHO: DEPARTURE AND DISPOSAL IN THE BCR4BP

Baseline Trajectories

The halo family and its subset, the Near Rectinilear Halo Orbits (NRHOs), are three-dimensional periodic orbits in the Circular Restricted 3-Body Problem (CR3BP). The halo family bifurcates from the planar Lyapunov family in the vicinity of each coplanar libration point. For the CR3BP equilibrium points L_1 and L_2 in the Earth-Moon system, the halo family members originate in the $x-y$ plane after the bifurcation with the Lyapunov family, and evolve out of plane as they approach the Moon. The NRHO subset of the L_1 and L_2 halo families are defined by their linear stability properties.[6] The Earth-Moon L_2 halo family appears in Figure 5a.

The NRHO of interest in the current investigation is selected in part due to advantages for eclipse avoidance. Avoiding long eclipses due to Earth shadow is of particular interest for the Gateway. Eclipses due to the Earth occur when the Sun, Earth, and spacecraft are aligned. This configuration occurs every synodic period of the Moon, which is approximately 29.4873 days. In this investigation, a 9:2 NRHO (9 revolutions in the orbit per 2 synodic periods of the Moon) is the baseline trajectory and, with appropriate phasing, eclipses due to Earth are avoided and lunar eclipses are rare. The 9:2 NRHO has a period of about 6.52 days and a perilune radius of 3157.8 km. Since the lunar radius is about 1737 km, the 9:2 NRHO, colored in black in Figure 5a, is accessible.

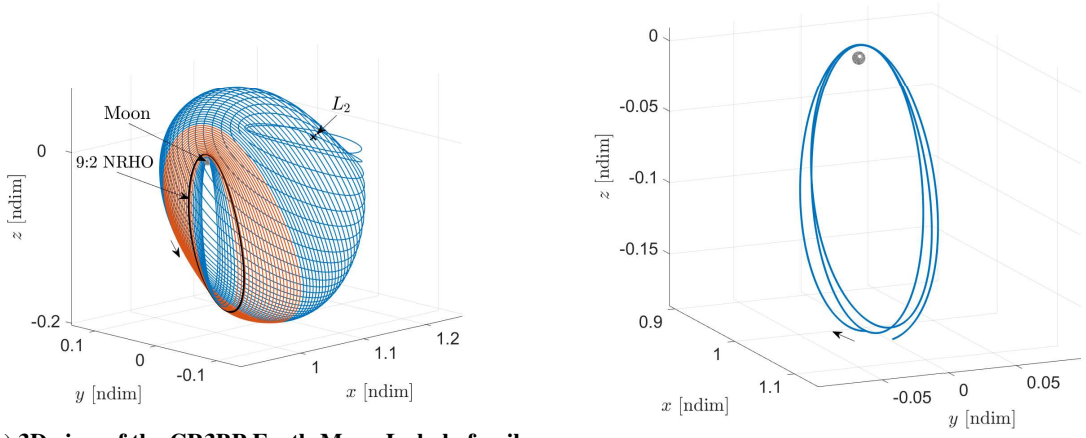

(a) **3D view of the CR3BP Earth-Moon L_2 halo family. The NRHO subset members are colored in orange. The 9:2 NRHO is plotted in black.**

(b) **The 9:2 NRHO reconverged in the BCR4BP.**

Figure 5: **Baseline Trajectories in the E-M rotating frame**

In the BCR4BP, the NRHOs are not perfectly periodic, but the geometry can be maintained. Stacking multiple revolutions of selected CR3BP NRHOs and employing a corrections scheme to enforce continuity yields a continuous trajectory that maintains the geometry of the NRHO for a certain time. This stacking procedure is typically employed to transition a periodic orbit from the CR3BP to the ephemeris model;[7] it is also applicable when transitioning from the CR3BP to the BCR4BP. A non-homogeneous[8] stacking technique is applied to regulate the BCR4BP NRHO perilune radius. A differential corrections scheme is then used to reduce position and velocity discontinuities between consecutive arcs to an acceptable tolerance. The NRHOs reconverged in the BCR4BP preserve the original geometry and the altitude of the periapses, as observed in Figure 5b.

Departure

The momentum integral[9] is a suitable metric to detect departure of the spacecraft from the NRHO. The momentum integral is a line integral for the position vector between the initial time t_0, and the current time, t:

$$\mathrm{MI}_{\Gamma}(t) = \int_{t_0}^{t} x(\tau)\dot{x}(\tau) + y(\tau)\dot{y}(\tau) + z(\tau)\dot{z}(\tau)\, d\tau \tag{7}$$

where x, y, z are the position vector ($\bar{x}_{B_1}^{E-M\ \text{Rotating}}$) components in the Earth-Moon rotating frame, $\dot{x}$, $\dot{y}$, $\dot{z}$ are the velocity vector components in the same frame, and τ is an independent time variable. The momentum integral over one period along a perfectly periodic orbit in the CR3BP is zero. In time-dependent models, such as the BRC4BP and the ephemeris model, the trajectory is not likely to precisely return to the initial state. Therefore, the momentum integral is not zero, but it remains bounded if the motion is bounded. To determine if the spacecraft has departed the NRHO, the momentum integral of the perturbed trajectory $\tilde{\Gamma}$ is evaluated and compared to the momentum integral for the reference trajectory Γ. In the current analysis, the reference trajectory Γ is selected as the NRHO without stationkeeping, and the perturbed trajectory $\tilde{\Gamma}$ is defined as the spacecraft trajectory with a disposal maneuver applied. The instantaneous difference between

their momentum integrals is defined as follows,

$$\Delta \text{MI}(t) = |\text{MI}_{\Gamma}(t) - \text{MI}_{\tilde{\Gamma}}(t)| \tag{8}$$

The perturbed trajectory remains in the vicinity of the reference trajectory for small ΔMI. Each application of the momentum integral employs a unique value for the metric. For this investigation, the spacecraft is considered departed from the NRHO when the values of ΔMI exceeds 10^{-1}.

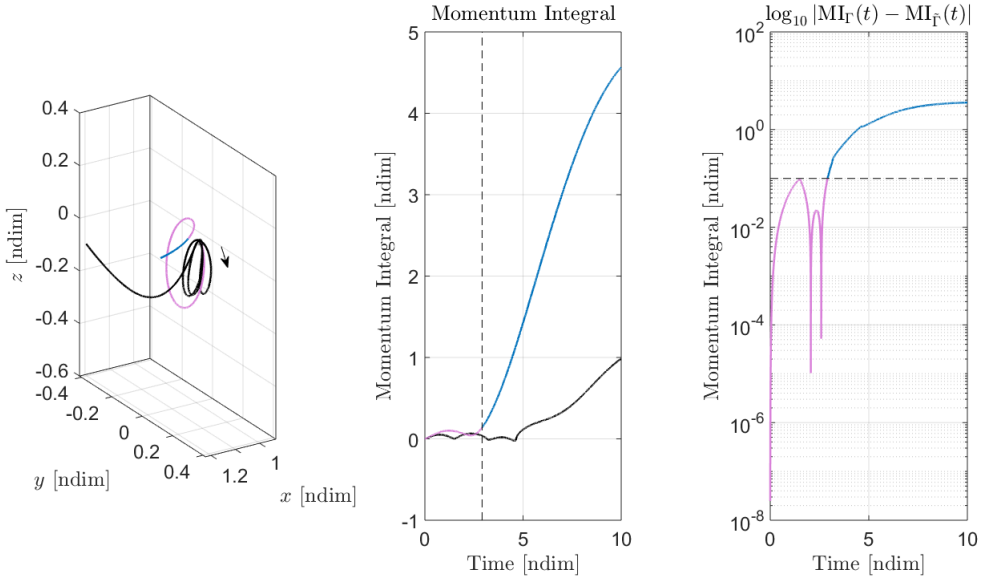

Figure 6: **Application of the Momentum Integral to define departure in the BCR4BP. The baseline trajectory is plotted in black. The actual trajectory, with a ΔV of 12 m/s implemented at the perilune, is colored in pink when it remains in the vicinity of the NRHO, and in blue when it has departed from the NRHO. Note that the baseline also leaves the NRHO at a later date since no stationkeeping is implemented.**

Disposal Framework

Definitions

The goal of the current disposal analysis is escape of the spacecraft from the Earth-Moon vicinity such that the vehicle enters and remains in heliocentric space. The Earth-Moon vicinity is defined as the region inside the CR3BP Sun-B_1 Hill region, that is, the sphere centered at the Earth-Moon barycenter (B_1) of radius approximately equal to the L_1 distance defined in the Sun-B_1 CR3BP. The Earth vicinity is the region within the sphere centered at the Earth with a radius approximate equal to the L_1 distance as defined in the Earth-Moon CR3BP. An escape, also denoted a 'success', is a trajectory which meets the following conditions after propagation for 365 days:

- Remains beyond the Earth vicinity.
- Crosses the boundary identifying the Earth-Moon vicinity only once (to exit and not return).

A capture (also labeled a 'failure' in this investigation) occurs when a trajectory does not satisfy at least one of these conditions. Heliocentric space is the region exterior to the Earth-Moon vicinity and interior to the Sun orbit in the E-M rotating frame. The Earth-Moon vicinity and the Earth vicinity appear in the Earth-Moon rotating frame and in the Sun-B_1 rotating frame in Figure 7.

Quadrants

In the $S - B_1$ rotating frame, the direction of the net perturbing acceleration due to the Sun, denoted the tidal acceleration, on a spacecraft in an orbit about the B_1 i.e., the Earth-Moon barycenter, depends on

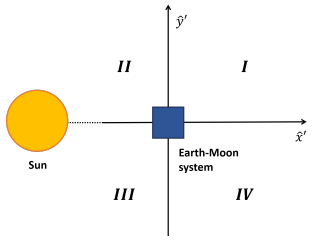

Figure 8: **Quadrants as defined in the $\mathbf{S - B_1}$ rotating frame**

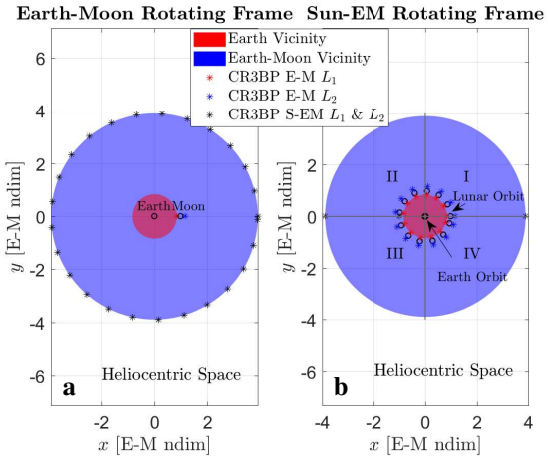

Figure 7: **The Earth-Moon vicinity, the Earth vicinity, and heliocentric space in the Earth-Moon rotating frame (a) and the Sun-B_1 rotating frame (b).**

the orientation of the orbit relative to the Sun and the Earth-Moon system. A set of quadrants, centered at B_1 is defined to facilitate the investigation of the tidal acceleration.[10] The quadrants are defined in the $S - B_1$ rotating frame, as illustrated in Figure 8. When the spacecraft orbit is viewed in the $S - B_1$ rotating frame, its orientation is defined by the quadrant that includes the apoapsis along a given revolution. The effects of the tidal acceleration are greatest near apoapsis. Assuming a prograde orbit:

- In quadrants I and III, the perturbations generally oppose the direction of the motion. As a result, solar effects tend to tend to elongate the orbit and decrease the periapse radius.
- In quadrants II and IV, the perturbations are generally along the direction of the motion. The orbit tends to circularize and the periapse tends to increase.

The location of a trajectory's apoapses within the quadrants are thus affected by the Sun's tidal effects. However, it should be noted that the Sun's perturbing effect is the largest on a spacecraft moving in the Sun-B_1 plane, while the disposal trajectory may possess non-zero z' components.

RESULTS IN THE BCR4BP

Multiple factors influence the disposal trajectory and the assessment as a success (escape) or a failure (capture). These effects include: the location of a trajectory apoapsis within the quadrants, the energy of the trajectory, and the orbit's osculating eccentricity with respect to B_1.To escape the Earth-Moon vicinity, the Sun-B_1 portals near L_1 and L_2 must be open, so the energy level H of the trajectory must be below the one of L_1 (if escaping through L_1) or of L_2 (if escaping through L_1 or L_2). The same reasoning applies for the osculating eccentricity with respect to B_1 if the eccentricity is less than 1, the trajectory is captured around B_1 if the eccentricity drifts above 1, the trajectory is hyperbolic with respect to B_1 in the Keplerian sense. Factors that do not significantly influence the escape include the altitude of the perilune or the magnitude of the ΔV maneuver. While increasing the ΔV magnitude tends to decrease the time to depart the NRHO, it does not guarantee an escape: escapes are found for $\Delta V = 1$ m/s and captures occur at $\Delta V = 100$ m/s. These elements reaffirm that the disposal problem is a Sun-B_1 problem.

The chronology of the disposal is repeated here. The disposal ΔV maneuver is performed at perilune on the NRHO in the rotating velocity direction. Depending on the magnitude of the ΔV, the spacecraft may or may not perform any post-maneuver revolutions on the NRHO. Once departed from the NRHO, the spacecraft is in the Earth-Moon vicinity. Depending on the factors outlined in the previous paragraph, the trajectory will do one of the following:

- **Direct Escape:** Directly catch the departing flow.

- **Indirect Escape:** Have additional E-M apopases but eventually catch the departing flow.
- **Capture:** Have additional E-M apopases but do not catch the departing flow, or impact the Moon/the Earth.

Each outcome is detailed in the next subsections.

Direct Escape

Direct escape trajectories directly leave the Earth-Moon vicinity after departing the NRHO. These direct escapes are allowed by the fact that they have the correct energy level once departed from the NRHO, meaning the $S - B_1$ gateways are open. An example of direct escape is provided in Figures 9 and 10. In this example, a maneuver of magnitude $\Delta V = 1$ m/s is implemented at perilune in the rotating $E - M$ velocity direction. The spacecraft performs 4 additional revolutions on the NRHO before departing (in all the following figures, lines colored in pink indicates the spacecraft is still on the NRHO, because $\Delta\text{MI}(t) < 10^{-1}$). Four apoapses with respect to B_1 marked by red dots and numbered in Figures 9 and 10, occur during the post-maneuver revolutions.

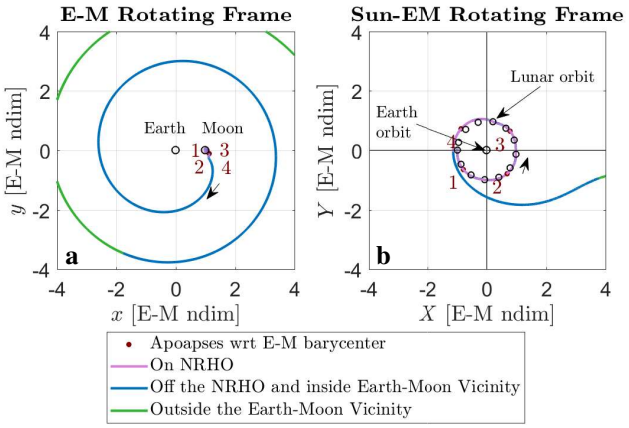

Figure 9: **A direct escape for $\Delta\mathbf{V} = 1$ m/s in the BCR4BP, as seen in the $\mathbf{E - M}$ rotating frame (a) and the $\mathbf{S - B_1}$ rotating frame (b).**

Once the spacecraft departs the NRHO, it is moving in Earth-Moon space. In the all the following figures, the lines corresponding to the spacecraft off the NRHO but still inside the Earth-Moon vicinity are colored in blue. The lines corresponding to the spacecraft off the NRHO and outside the Earth-Moon vicinity (in heliocentric space) are colored in green. In Figure 9a, the trajectory can be seen escaping the Earth-Moon vicinity through the instantaneous $S - B_1L_2$. The energy history of the trajectory, presented in Figure10, indicates that L_1 and L_2 are open when the spacecraft depart the NRHO. Note that energy is constant after the spacecraft escapes the Earth-Moon vicinity. In heliocentric space, the influence of the Earth and the Moon circular motion on the spacecraft trajectory is minimal; the BCR4BP energy can be approximated by the CR3BP Sun-B_1 Jacobi Constant.

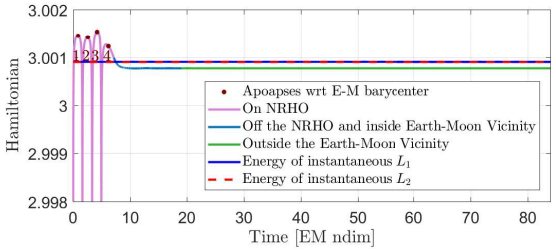

Figure 10: **Energy history of the direct escape trajectory in the $\mathbf{S - B_1}$ frame**

Indirect Escape

Indirect escapes have at least one additional apoapse with respect to the Earth-Moon barycenter,B_1, before escaping the Earth-Moon vicinity. The tidal effects from the Sun change the energy and the eccentricity of the trajectory, which is then able to escape. An example of indirect escape is presented in Figure 11 and 12. A disposal maneuver of manitude $\Delta V = 7$ m/s is implemented at the first perilune. Because the maneuver

magnitude is higher than in the previous example (Figure 9), the spacecraft performs only two post-maneuver revolutions on the NRHO before departure.

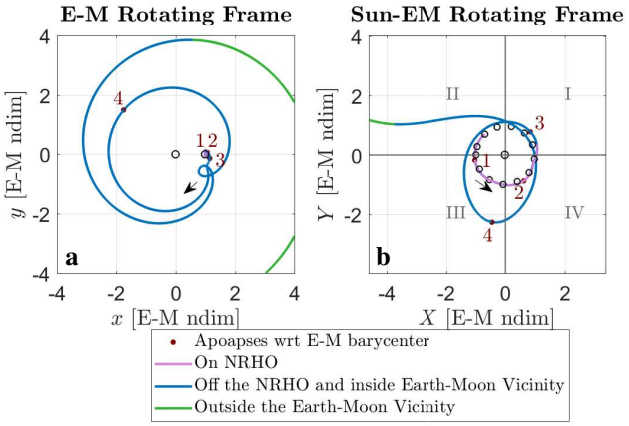

Figure 11: **An indirect escape for $\Delta V = 7$ m/s in the BCR4BP, as seen in the $E - M$ rotating frame (a) and the $S - B_1$ rotating frame (b).**

The first two apoapses, labeled 1 and 2, occur while the spacecraft is still on the NRHO, therefore, they are not included in the tidal effect analysis. At the third apoapse, the spacecraft has departed from the NRHO. This apoapse and the following, 4, are located in quadrant I and quadrant III respectively. Recall that in these two quadrants, perturbations generally oppose the direction of the motion of a prograde orbit. The osculating eccentricity increases after apoapses 3 and 4, as shown of Figure 12b. After periapse 4, the osculating eccentricity surpasses one, the trajectory is now hyperbolic with respect to the Earth-Moon barycenter, B_1 and the spacecraft escapes the Earth-Moon vicinity. The energy of the trajectory in the Sun-B_1 frame, presented in Figure 12a, is also insightful. After departure from the NRHO, the energy is too low (equivalently, H is too high) and both the instantaneous L_1 and L_2 are closed. The energy increases after apoapse 3 and apoapse 4; after the last apoapse, the energy is higher than the energy of the instantaneous L_1 and L_2 and the spacecraft escapes.

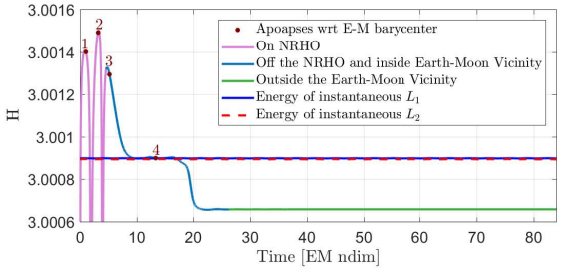

(a) **Energy history of the indirect escape trajectory in the $S - B_1$ frame**

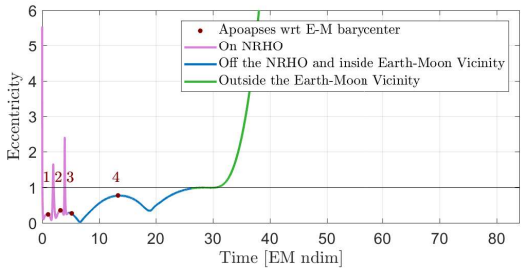

(b) **Osculating eccentricity with respect to B_1 of the indirect escape trajectory in the $S - B_1$ frame. The black line indicates the eccentricity equal to 1.**

Figure 12: **Indirect escape trajectory energy and osculating eccentricity in the Sun-B_1 rotating frame**

Capture

Captures do not escape in the one-year timespan, or they enter the vicinity of the Earth, the sphere centered at B_1 of radius approximately equal to the Earth-Moon CR3BP L_1 distance. The captures have an energy level when they depart the NRHO such that the instantaneous L_1 and/or L_2 are closed. An example of capture is presented in Figures 13 and 14. Lunar flybys modify the trajectory dynamics and can potentially offset the tidal effect gained at the apoapses. After apoapse 3, the spacecraft enters the Earth-Moon vicinity, as in Figure 13: the trajectory is therefore categorized as a capture. The trajectory is propagated after apoapse 3 to investigate whether an escape occurs. Though the tidal effects and flybys of the primary act on the spacecraft, the trajectory never achieves the correct combination of eccentricity, energy, and orientation to escape. Additionally, the spacecraft falls into a resonant structures with close passes to the Earth, as in Figure 13(left). The flybys of the Earth are characterized by the peaks in energy H in Figure 14a between apoapses 6 and 7, apoapses 9 and 10, and after apoapse 10. In this example, the spacecraft escapes the Earth-Moon

vicinity after over 2 years with multiple lunar and Earth flybys; this trajectory does not qualify as a safe disposal option.

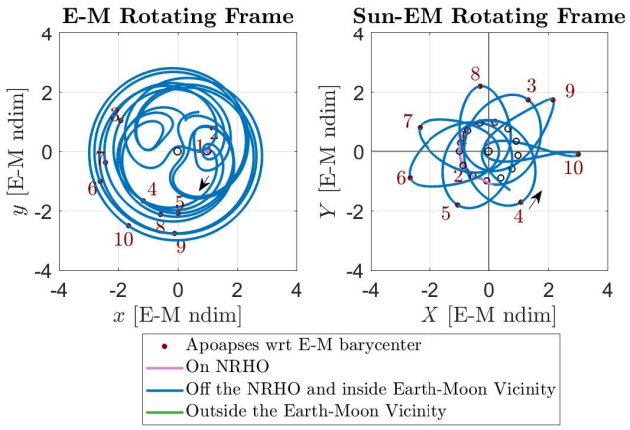

Figure 13: **A capture trajectory propagated for 1.25 years with a disposal maneuver $\Delta V = 7$ m/s in the BCR4BP, as seen in the $E - M$ rotating frame (a) and the $S - B_1$ rotating frame (b).**

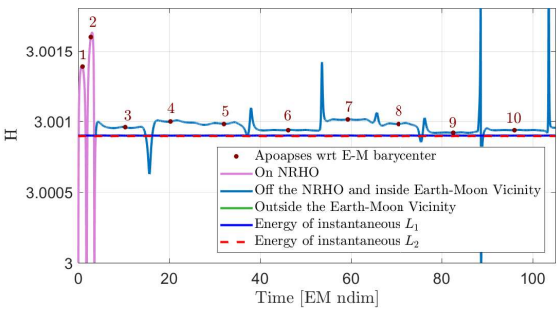

(a) **Energy history of the capture trajectory in the $S - B_1$ frame**

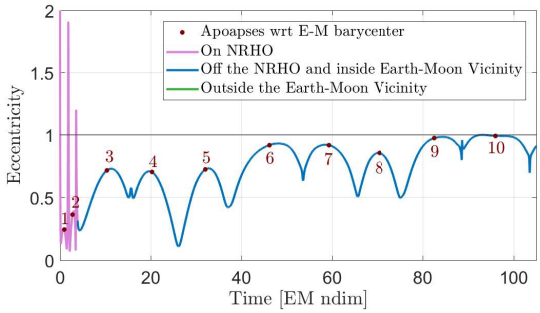

(b) **Osculating eccentricity with respect to B_1 of the capture trajectory in the $S - B_1$ frame. The black line indicates the eccentricity equal to 1.**

Figure 14: **Indirect escape trajectory energy and osculating eccentricity in the Sun-B_1 rotating frame**

NRHO: DEPARTURE AND DISPOSAL IN THE EPHEMERIS MODEL

Predictions from the BCR4BP effectively describe trajectory behavior and trends in the ephemeris force model. These predictions are applied to Gateway mission scenarios in the higher-fidelity ephemeris model to generate specific examples of successful LM disposal scenarios. First, the problem is framed in terms of the reference NRHOs employed in the analysis. The post-maneuver time to NRHO departure is explored, and then sample scenarios representing direct escape, indirect escape, and capture are generated.

Baseline Trajectories

Properties of disposal trajectories in the sensitive cislunar regime, in which the gravitational effects of the Sun, Earth, and Moon are simultaneously significant, depend on the quality of the reference NRHO trajectory. Employing a well-converged reference trajectory in the analysis is important to ensure the spacecraft is not

already on a path departing from the NRHO before the disposal maneuver is applied. For the current analysis, long-horizon reference NRHOs are generated in the ephemeris model through a forward-backward shooting process that takes patch points from the CR3BP NRHO and converges them into the ephemeris force model.[11] As in the BCR4BP, the perfectly periodic CR3BP NRHO becomes a quasi-periodic NRHO in the ephemeris model, but it retains properties of the original periodic orbit. The primary reference orbit is a 9:2 lunar synodic resonant NRHO phased to avoid eclipses by the Earth. The reference trajectory extends for 15 years with an initial epoch in January 2020. Additional reference orbits are also examined to confirm that results are not specific to an individual reference NRHO; each extends for over a year in an approximate 9:2 resonance with the lunar synodic period. Starting epochs range from January 2020 to May 2023.

Prior to a disposal maneuver, the reference spacecraft is maintained in the NRHO via an x-axis crossing control orbit maintenance (OM) algorithm[7,9,12] with small burns at apolune. After the disposal, the spacecraft is ballistically propagated until departure from the NRHO is achieved and escape/capture outcomes are determined.

Departure

As demonstrated in the BCR4BP analysis, the location of the Sun after the spacecraft departs from the NRHO determines in part the long-term destination of the spacecraft. Thus, the epoch of departure from the NRHO is critical to the spacecraft's fate. Additionally, the more post-burn revolutions the spacecraft experiences in or near the NRHO, the more opportunity there is for small variations in the orbit to change the actual epoch of departure. Understanding the duration of time spent in the vicinity of the NRHO after a disposal maneuver is thus a key to designing disposal scenarios with the desired outcome. Multiple factors affect the time to depart the NRHO; factors include quality of the converged reference NRHO, maneuver location along the NRHO, and magnitude and direction of the disposal maneuver.

The first parameter explored is the quality or stability of the converged reference orbit in the ephemeris force model. That is, how long an uncontrolled spacecraft remains in the NRHO before departure, as defined by divergence of the momentum integral. To quantify the time to departure, the spacecraft is maintained in the NRHO in the presence of navigation errors, maneuver execution errors, wheel desaturation errors, and SRP errors as previously defined. After a given number of revolutions in the NRHO, the orbit maintenance is turned off and the spacecraft is propagated to departure. Fifty Monte Carlo trials are run for each of four cases, in which orbit maintenance ceases after 2, 3, 4, or 5 revolutions in the NRHO. The time histories of the MI for the 50 Monte Carlo trials in the final case appear in Figure 15. After 5 revolutions in the NRHO, represented in magenta, the final orbit maintenance maneuver (OMM) is performed at apolune and each trajectory is propagated forward uncontrolled, as shown in blue. After about 6 more revolutions near the NRHO, the 50 trials start to diverge from one another. The first trial to depart the vicinity of the NRHO does so 56.7 days after OM is ceased, or after 8 additional revolutions near the NRHO. The final trial to depart remains in the vicinity of the NRHO for 102.9 days, almost twice as long. The minimum, mean, and maximum times to depart in the four cases appear in Table 1 highlighted in blue. The mean times to escape are relatively consistent, ranging from 72.4 days to 78 days in the NRHO vicinity. However, the mean and maximum times to escape vary widely. Additionally, time to depart a poorly-converged NRHO is significantly faster. Without a disposal maneuver, the epoch of departure from the vicinity of the NRHO (and hence the final destination of the departing spacecraft) is unpredictable based on the time of OM cessation. A sample trajectory that escapes after 68.5 days appears in Figure 15b.

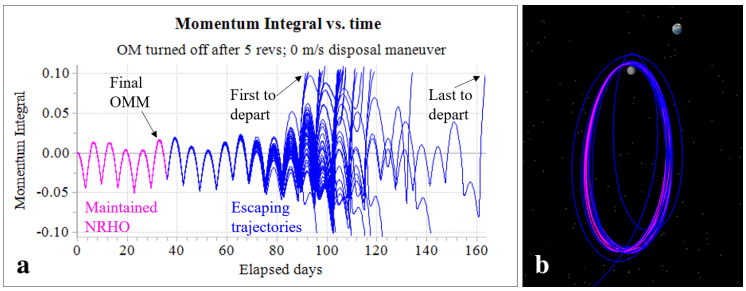

Figure 15: **Momentum Integral histories for 50 Monte Carlo trials with no disposal maneuver (a), sample escaping orbit (b)**

Table 1: **Days to NRHO Departure. OM for 2-5 revolutions, 50 Monte Carlo trials per case**

	Days to NRHO Departure											
	0 m/s disposal			1 m/s disposal			5 m/s disposal			15 m/s disposal		
rev	min	mean	max	min	mean	max	min	mean	max	min	mean	max
2	55.6	74.7	114.2	31.8	37.2	39.5	17.3	17.4	17.5	13.5	13.6	13.8
3	59.3	76.2	107.7	30.6	30.9	31.2	16.9	17.0	17.0	13.0	13.1	13.1
4	56.7	72.4	102.9	30.7	32.4	37.7	18.1	18.3	18.4	12.3	12.3	12.4
5	56.6	72.4	121.7	30.0	30.6	38.0	17.6	17.8	17.9	12.9	13.0	13.0

The time to depart the NRHO is significantly more consistent when a disposal maneuver is applied, however, the maneuver location along the NRHO has a substantial impact on departure time. In general, an NRHO is most sensitive to perturbations near perilune. Thus, for a spacecraft in long-term operations in an NRHO, perturbations near the Moon are to be avoided. However, for a spacecraft departing the NRHO, a disposal maneuver near perilune is the most effective for fast departure from the orbit. To characterize the dependency of departure time on maneuver location, a set of departure cases is run for maneuvers at various values of true anomaly (TA) around multiple revolutions the NRHO. In each case, a 1 m/s burn in the velocity direction is applied to the spacecraft, which is then propagated to NRHO departure. Stepping along the NRHO in 5° increments, the process is carried out for nine revolutions of the NRHO. The results appear in Figure 16a. The maximum escape times consistently occur just prior to apolune. Surrounding apolune, at values of TA between approximately 130° and 210° times to depart the NRHO vary considerably from one TA to the next; that is, a small change in maneuver TA leads to a large difference in departure time. Spikes in the trends are visible around 60° and 270°.These spikes correspond to trajectories that make several large additional revolutions around the Moon prior to departing. In contrast, prior to perilune, departure times are consistently about 30-32 days, with the exception of the maneuver after two revolutions, which remains in the NRHO for an extra revolution. For maneuvers near perilune, small variations in maneuver TA do not significantly alter the time to depart. For predictable departure times, maneuvers near perilune are the most consistent.

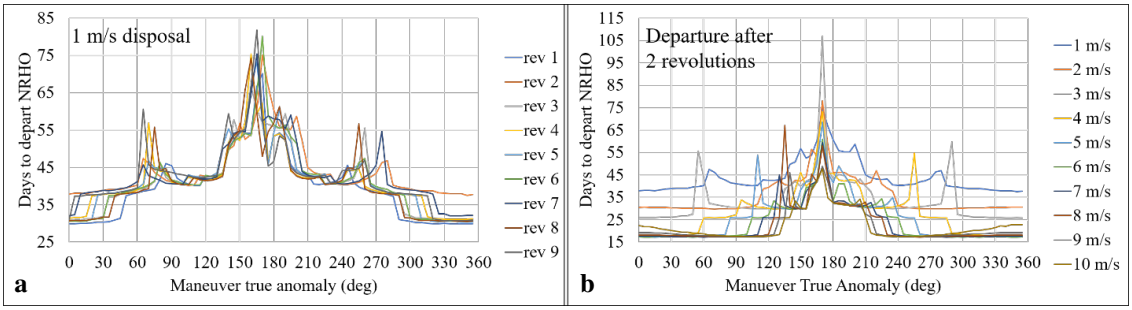

Figure 16: **Days to depart the NRHO as a function of maneuver TA around nine revolutions of the NRHO after a 1 m/s disposal burn (a). Days to depart the NRHO as a function of maneuver TA after 2 revolutions for varying maneuver magnitudes (b).**

From this point onward, the disposal maneuver is assumed to occur at perilune, and trends in departure time as a function of maneuver magnitude are investigated. In general, as the size of the disposal burn increases, the time to depart decreases, but the pattern is not linear. For maneuver magnitudes ranging from 1 m/s to 20 m/s, Monte Carlo analyses are run for departure burns after 2, 3, 4, and 5 revolutions in the NRHO. Fifty trials are run per case with navigation and spacecraft errors applied as previously described. Minimum, mean, and maximum times to departure from the NRHO for each case appear in Figure 17. Results are relatively

consistent, though some variations are apparent. The times to depart without a maneuver, as previously noted, are large and vary considerably between trials. The time to depart quickly falls and becomes more consistent as a maneuver is added. As the maneuver size increases, the time to depart tends to decrease as a step function, with the escape occurring after a discrete number of revolutions near the NRHO. Depending on the specific perilune within the reference NRHO that contains the disposal maneuver, the step down to a lower departure time occurs at different maneuver magnitudes. The minimum, mean, and maximum times to escape for 1 m/s, 5 m/s, and 15 m/s disposal burns appear in Table 1.

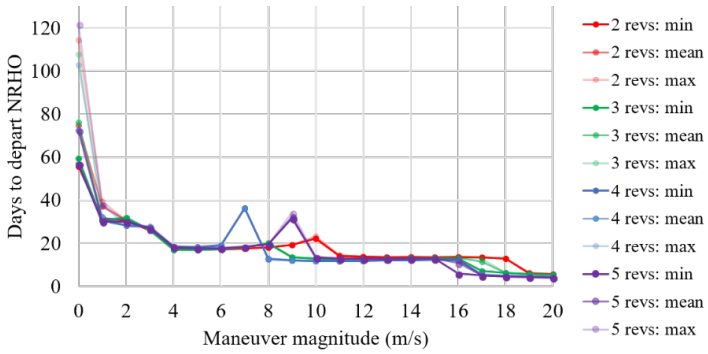

Figure 17: **Minimum, mean, and maximum times to departure for a range of disposal maneuver magnitudes after 2, 3, 4, or 5 revolutions in the NRHO.**

Finally, to complete the exploration of the departure behavior, single Monte Carlo trials are run for various maneuver magnitude values applied consecutively over 63 revolutions or the NRHO. That is, a 1 m/s disposal burn is applied after the first revolution in the NRHO and propagated to departure. The process is repeated by applying a disposal burn after two revolutions in the NRHO and propagating to departure, then after three revolutions, four, and so on until in the final case, the spacecraft spends 63 revolutions, or 447 days, orbiting in a maintained NRHO prior to the departure maneuver. In each case, the time to depart is recorded and consistency is examined across the disposal maneuver epochs. Departure times for six selected values of disposal burn magnitude appear in Figure 18. For some burn magnitudes, including 2 m/s, 5 m/s, and 15 m/s, the time from disposal burn to NRHO departure is consistent across the 63 revolutions. For other values of disposal burn magnitude, including 1 m/s, 7 m/s, and 17 m/s the departure time has variations for certain disposal burn revolutions. Figure 18a corresponds to the baseline 15-year 9:2 lunar synodic resonant NRHO, with an initial epoch in January 2020. The process is repeated for a second reference trajectory to assess the dependence of results on a particular reference NRHO. The second reference is also in a 9:2 resonance with the lunar synodic period, but it is not phased to avoid eclipses, and it has an initial epoch in May 2023. The patterns in the time to depart the NRHO are consistent across all but the lowest value of maneuver magnitude. For a burn with a maneuver magnitude of 1 m/s, the secondary reference trajectory demonstrates a consistent time of departure of just over 40 days (Figure 18b), while the primary reference orbit departs faster, usually in around 30 days.

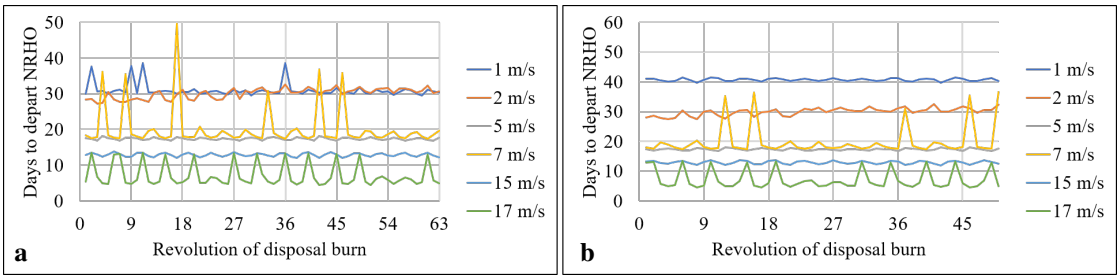

Figure 18: **Time to NRHO departure measured from the disposal burn for several ΔV magnitudes. Disposal burn occurs after 1 to 63 revolutions within the NRHO. Baseline reference NRHO (a) and secondary reference NRHO (b).**

RESULTS IN THE EPHEMERIS MODEL

For LM disposal from the Gateway, direct escapes to heliocentric space are of interest to avoid threatening assets either at the Moon or Earth. As in the BCR4BP, the spacecraft's energy, location within the quadrants, and osculating eccentricity affect the outcome of the disposal. The time to depart the NRHO combined with the epoch of the departure burn determine the location of the departing trajectory within the quadrants in the Sun-B_1 frame. Samples of direct escapes to heliocentric space, indirect escapes, and captured trajectories that remain Earthbound illustrate the applicability of the BCR4BP analysis in the higher-fidelity ephemeris model.

Direct Escape

Disposal trajectories that directly escape into heliocentric space are candidate end-of-mission paths for LMs. One example appears in Figure 19. After two revolutions of orbit maintenance in the NRHO, a disposal maneuver of 1 m/s in the velocity direction is executed at perilune. Ten sample Monte Carlo trials appear in the Sun-B_1 rotating frame in Figure 19a and in the Earth-Moon rotating frame in Figures 19b and 19d. The magenta curve represents the maintained revolutions in the NRHO. The blue portions of the trajectories correspond to post-maneuver revolutions in the Earth-Moon vicinity. The color changes to green when the trajectories escape the Hill region associated with the Earth. In Figure 19b, the revolutions in the maintained NRHO and the post-maneuver revolutions near the Moon are apparent looking down the x-axis towards the Earth in the Earth-Moon rotating frame. In Figure 19d, a wide, top-down view of the Earth-Moon rotating frame shows the escape from the Earth-Moon vicinity. The trajectories diverge slightly over time due to small differences in their post-disposal maneuver states, but they all exit the vicinity of the Earth to heliocentric space. Each trajectory passes through its final perigee quadrant III in the Sun-B_1 rotating frame (marked by a white arrow in Figure 19a), elongating the orbit as it escapes the Earths vicinity through Sun-B_1 L_2 . In Figure 19c, the Sun-B_1 Jacobi constant appears as a function of time. The Jacobi values associated with the Sun-B_1 L_1 and L_2 libration points appear as a black line, indistinguishable at this scale. As the spacecraft departs the NRHO, its Jacobi constant lies below that associated with Sun-B_1 L_2 (Figure 19b), providing for open ZVCs at L_2 that allow escape from the Earth-Moon region. Because the propagations occur in the ephemeris force model, the value of Jacobi is not constant, as it would be in the Sun-B_1 CR3BP. The large perturbations to the Jacobi value by the Moon are readily apparent as spikes in the magenta and blue revolutions near the Moon for the first 50 days. The Jacobi trend flattens as the spacecraft departs the vicinity of the Moon, but it grows slightly over time due to the eccentricity of the Earths orbit, eventually closing off the ZVCs at L_2 .

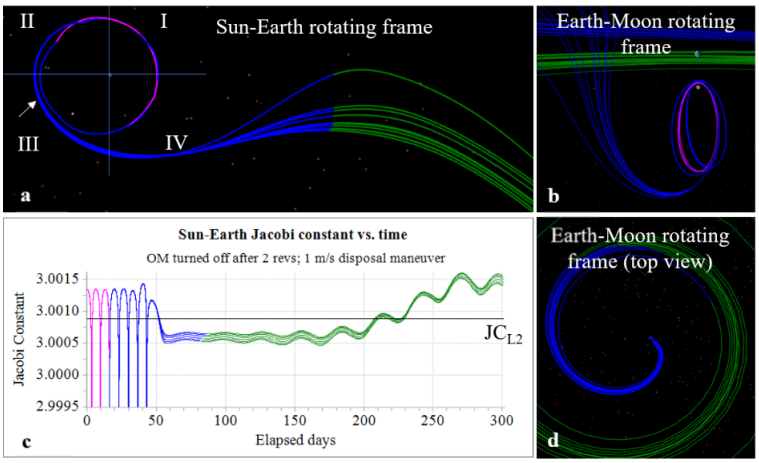

Figure 19: **Direct escapes in the Sun-B_1 rotating frame with a 1 m/s burn after 2 revolutions in the NRHO (a), Evolution of the Sun-B_1 Jacobi constant over time (c), direct escapes in the Earth-Moon rotating frame (b), (d).**

Indirect Escape

As in the BCR4BP, the complex dynamics affecting the post-departure regime in the ephemeris model lead to certain trajectories escaping not immediately, but after several revolutions around the Earth. One such example appears in Figure 20. In this example, a 5 m/s disposal maneuver is applied in the velocity direction at perilune after four revolutions in the NHRO. Ten sample Monte Carlo trials are propagated forward, and none escapes immediately from the vicinity of the Earth. The post-maneuver revolutions in the vicinity of the Moon are visible in blue in Figure 20b. After passing perigee in quadrant III, as in Figure 20a, each continues to orbit the Earth, passing through apogee in quadrant I, marked by a white arrow in Figure 20a. The additional revolutions around the Earth appear in the Earth-Moon rotating frame in Figure 20d. Eight of the sample orbits then escape via Sun-B_1 L_2 . However, two of the trajectories, characterized by a slightly higher Jacobi value than the others and marked with a blue arrow in Figure 20a, remain bounded at Earth and do not escape. In a zoomed view of the Jacobi constant over time in Figure 21, the local maximum marked with a green arrow corresponds to the perigee passage in quadrant III immediately prior to either escape or continued capture around the Earth, also marked with a green arrow in Figure 20a. At this perigee passage, the Jacobi value of the escaping trajectories is below the value associated with L_1, while the Jacobi value of the captured trajectories is higher than the L_1 threshold. Note the higher values of Jacobi constant across each of the trajectories in Figure 20c, as compared to the previous example. With a Jacobi value very nearly equal to that associated with L_2, the ZVCs are nearly closed, and small differences in the post-maneuver state caused by spacecraft and navigation errors lead to inconsistent escape behavior. Other examples with disposal maneuvers of larger magnitude demonstrate the same inconsistent behavior in indirect escape scenarios. Direct escapes demonstrate a more consistent pattern than indirect escapes, and thus are better suited for robust LM disposal to heliocentric space.

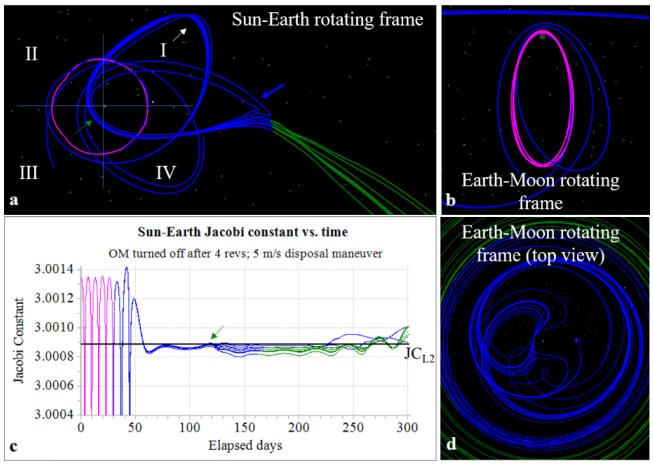

Figure 20: **Indirect escapes in the Sun-B_1 rotating frame with a 5 m/s burn after 4 revolutions in the NRHO (a), Evolution of the Sun-B_1 Jacobi constant over time (c), indirect escapes in the Earth-Moon rotating frame (b), (d).**

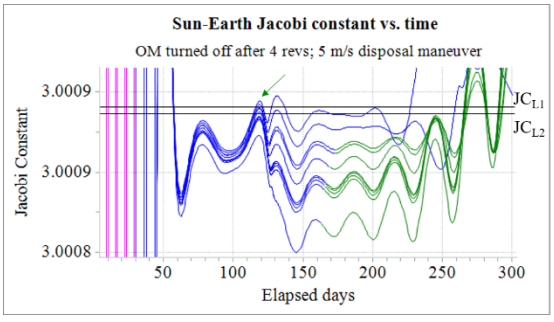

Figure 21: **Zoomed view of the Jacobi constant over time for indirect escapes and captures**

Capture

When the post-departure orientation is not appropriately aligned or the trajectory is insufficiently energetic, the trajectory remains bounded in the Earth-Moon system. A sample case appears in Figure 22. Ten sample Monte Carlo trials are performed by applying a 2 m/s disposal burn after 2 maintained revolutions in the NRHO. While each trajectory passes through apses in quadrants I and III, as apparent in Figure 22a, the Jacobi constant is never sufficiently low to allow escape through the ZVCs at either L_1 or L_2. That is, the Jacobi constant in Figure 22c remains always above the black line representing the Jacobi value corresponding to L_1 libration point in the Sun-B_1 system. The views in the Earth-Moon rotating frame in Figure 22b and 22d show the trajectories remaining bounded in the Earth-Moon vicinity.

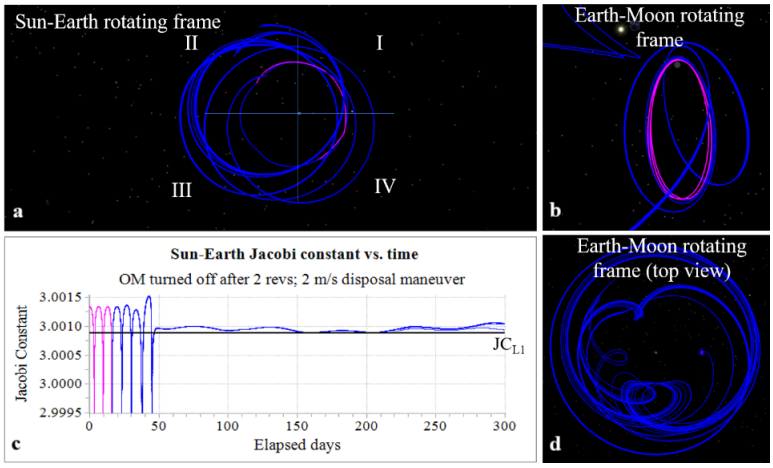

Figure 22: **Captured orbits in the Sun-B_1 rotating frame with a 2 m/s burn after 2 revolutions in the NRHO (a), Evolution of the Sun-B_1 Jacobi constant over time (c), captures in the Earth-Moon rotating frame (b), (d).**

Impacts

In some cases, disposal maneuvers applied at perilune result in impact with the Moon or the Earth. Lunar impact can occur prior to departure from the vicinity of the Moon, or the LM can depart from the Moon's vicinity and then re-enter the lunar vicinity and impact. Two examples appear in the Earth-Moon rotating frame in Figure 23. The first example, in Figure 23a, represents an impact after the disposal maneuver but before departure from the vicinity of the Moon. Such impacts are not observed for disposal maneuvers at perilune in the velocity direction; instead, direct impacts are observed for maneuvers in the anti-velocity direction in certain cases. The impact orbit in Figure 23a occurs when a disposal maneuver of 15 m/s in the anti-velocity direction is applied at perilune after four maintained revolutions in the NRHO. After the disposal maneuver, the LM continues in orbit around the Moon for two more revolutions, after which it impacts the Moon at perilune. In the second lunar impact example, appearing in Figure 23b, a 5 m/s disposal burn in the velocity

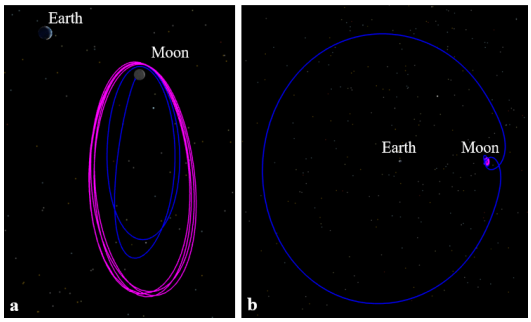

Figure 23: **Lunar impact trajectories in the Earth-Moon rotating frame. Direct impact after a 15 m/s maneuver in the anti-velocity direction (a), resonant orbit impact after a 5 m/s maneuver in the velocity direction (b).**

direction is executed after six maintained revolutions in the NRHO. The spacecraft exits the lunar vicinity in a resonant orbit with the Moons period around the Earth; two months later, it returns to the Moon on an impact trajectory.

Certain disposal trajectories that do not escape to heliocentric space are observed to impact the Earth. Two examples appear in the Sun-B_1 rotating frame in Figure 24. Both resemble ballistic lunar transfers (BLTs) in reverse. For a spacecraft departing from the Earth, BLTs employ solar gravity to raise perigee to the radius of the Moons orbit by placing apogee in quadrant II or IV. Whitley et al.[13] explore BLTs for Earth to NRHO transfers. In contrast, the two examples in Figure 24, starting from an NRHO and exiting the lunar vicinity with apogee in quadrants I and III, are affected by solar gravity such that the perigee is lowered to impact Earth. In Figure 24a, a maneuver of 17 m/s is applied in the velocity direction at perilune after two revolutions in the NRHO. An apogee in quadrant I leads to Earth impact at the subsequent perigee. Similarly, in Figure 24b, a maneuver of 10 m/s in the velocity direction is executed after two revolutions in the NRHO. After passing through apogee in quadrant III, the LM impacts Earth at its subsequent perigee. While unexpected impacts are to be avoided, these impact examples demonstrate that trajectories that intersect with both the Earth and Moon are available with low ΔV departure maneuvers. Such trajectories may be desirable for certain applications.

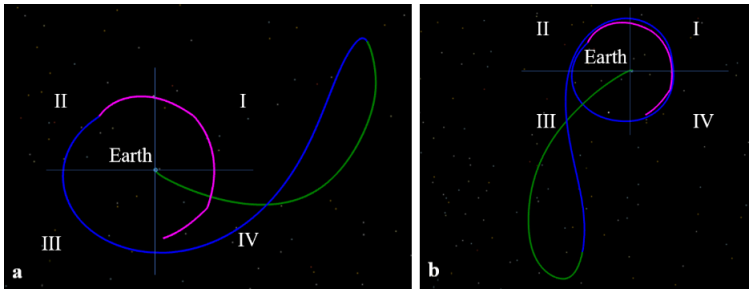

Figure 24: **Impacts with Earth in reverse ballistic lunar transfers after a 17 m/s disposal maneuver (a) and a 10 m/s disposal maneuver (b).**

CONCLUDING REMARKS

The investigation aims to leverage a bicircular 4-body model to gain better understanding of the escape dynamics in a solar-influenced disposal from an Earth-Moon NRHO. From the analysis in the BCR4BP, multiple factors influencing the disposal were found. First, the energy along the departure trajectory must be sufficiently high to allow escape through the Sun-B_1 L_1 or L_2 libration points. Second, the escaping trajectory must be appropriately oriented, with apses in quadrant I or quadrant III in the rotating Sun-B_1frame, to grant departure of the spacecraft. Finally, osculating eccentricity along the trajectory must be greater than one, signifying escape from the Earth-Moon vicinity.

Predictions from the BCR4BP effectively describe trajectory behavior in the higher-fidelity force model and are used to generate specific examples of successful Logistics Module disposal scenarios. Successful disposals to heliocentric space are presented for a disposal maneuver magnitude as low as 1 m/s.

ACKNOWLEDGMENT

This work was conducted at Purdue University and NASA Johnson Space Center under contract number NNJ13HA01C with some effort under cooperative agreement NNX13AK60A. The authors thank Ryan Whitley (JSC) and Andrew Cox (Purdue) for useful discussions. Also acknowledged is the Purdue University School of Aeronautics and Astronautics for facilities and support, including access to the Rune and Barbara Eliasen Visualization Laboratory.

REFERENCES

[1] K. Hambleton, "Deep Space Gateway to Open Opportunities for Distant Destinations," *NASA*, 2017.

[2] C. Warner, "NASA's Lunar Outpost will Extend Human Presence in Deep Space," *NASA*, 2018.

[3] G. Gómez, *Dynamics and Mission Design near Libration Points*, Vol. 2. World Scientific, 2001.

[4] J. Guzmán, *Spacecraft Trajectory Design in the context of a Coherent Restricted Four-Body Problem*. PhD dissertation, Purdue University, West Lafayette, IN, 2001.

[5] M. Andreu, *The Quasi-Bicircular Problem*. PhD dissertation, Universitat de Barcelona, 1999.

[6] E. Zimovan, K. Howell, and D. Davis, "Near Rectilinear Halo Orbits and Their Application in Cis-Lunar Space," *3rd IAA Conference on Dynamics and Controls of Space Systems, Moscow, Russia*, 2017.

[7] D. Davis, S. Philips, K. Howell, S. Vutukuri, and B. McCarthy, "Stationkeeping and Transfer Trajectory Design for Spacecraft in Cislunar Space," *AAS/AIAA Astrodynamics Specialist Conference Columbia River Gorge, Stevenson, Washington*, 2017.

[8] S. Vutukuri, "Spacecraft Trajectory Design Techniques Using Resonant Orbits," Master's thesis, Purdue University, West Lafayette, Indiana, 2018.

[9] D. Guzzetti, E. Zimovan, K. Howell, and D. Davis, "Near Rectilinear Halo Orbits and Their Application in Cis-Lunar Space," *27th AAS/AIAA Space Flight Mechanics Meeting, San Antonio, Texas*, 2017.

[10] D. Davis, *Multi-body Trajectory Design Strategies Based on Perioapsis Poincaré Maps*. PhD dissertation, Purdue University, West Lafayette, Indiana, 2011.

[11] J. Williams, D. Lee, R. Whitley, K. Bokelmann, D. Davis, and C. Berry, "Targeting Cislunar Near Rectilinear Halo Orbits for Human Space Exploration," *27th AAS/AIAA Space Flight Mechanics Meeting, San Antonio, Texas*, 2017.

[12] C. Newman, D. Davis, R. Whitley, J. Guinn, and M. Ryne, "Stationkeeping, Orbit Determination, and Attitude Control for Spacecraft in Near Rectilinear Halo Orbits," *AAS/AIAA Astrodynamics Specialists Conference, Snowbird, Utah, August 2018*, 2018.

[13] R. Whitley, D. Davis, M. McGuire, L. Burke, B. McCarthy, R. Power, and K. Howell, "Earth-Moon Near Rectilinear Halo and Butterfly Orbits for Lunar Surface Exploration," *AAS/AIAA Astrodynamics Specialists Conference, Snowbird, Utah, August 2018*, 2018.

APPENDIX

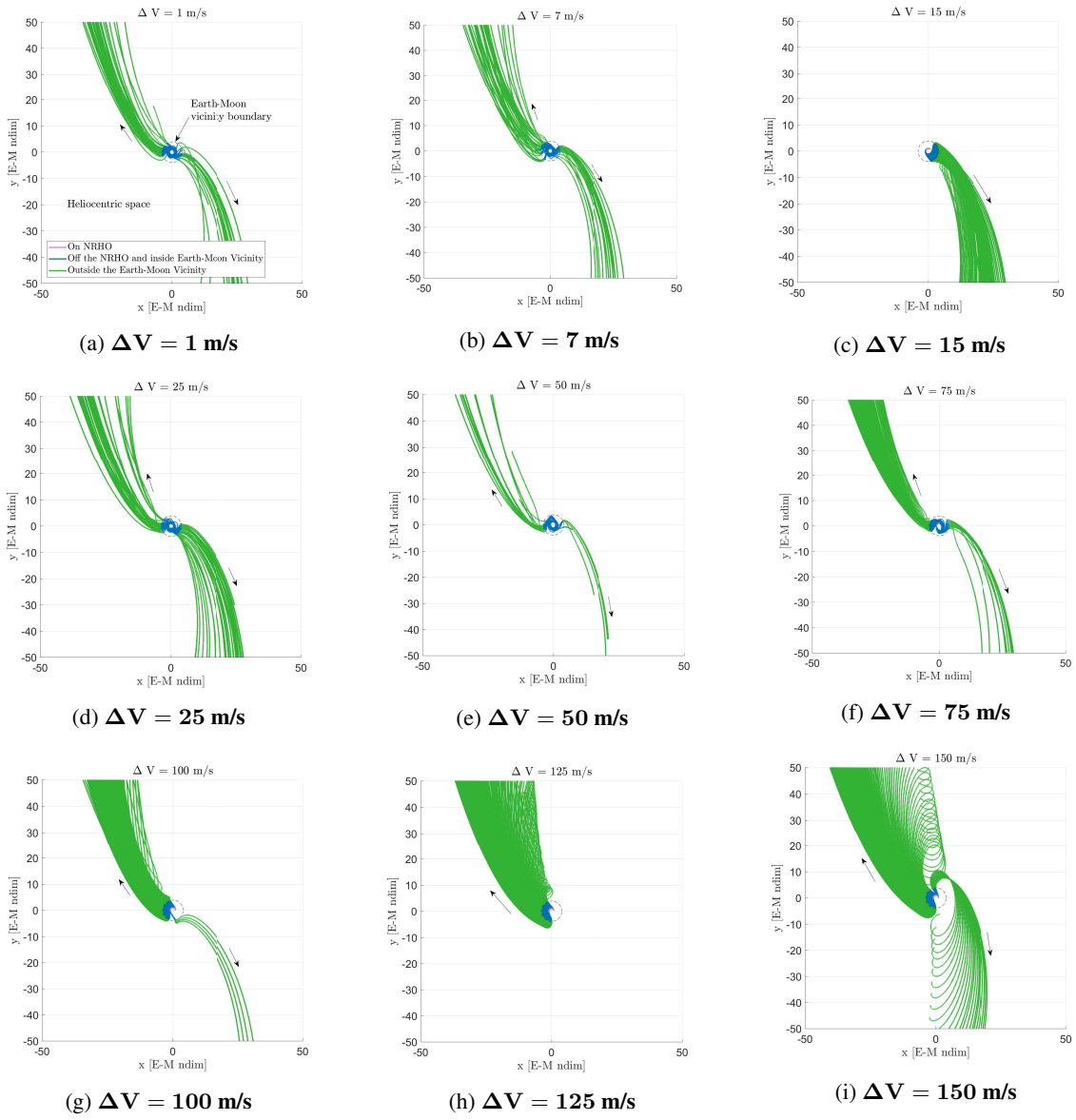

(a) $\mathbf{\Delta V = 1}$ **m/s** (b) $\mathbf{\Delta V = 7}$ **m/s** (c) $\mathbf{\Delta V = 15}$ **m/s**

(d) $\mathbf{\Delta V = 25}$ **m/s** (e) $\mathbf{\Delta V = 50}$ **m/s** (f) $\mathbf{\Delta V = 75}$ **m/s**

(g) $\mathbf{\Delta V = 100}$ **m/s** (h) $\mathbf{\Delta V = 125}$ **m/s** (i) $\mathbf{\Delta V = 150}$ **m/s**

Figure 25: **Indirect and direct escapes trajectories propagated for 365 years for a range of disposal maneuver $\mathbf{\Delta V}$ magnitude, as shown in the Sun-$\mathbf{B_1}$ rotating frame.**